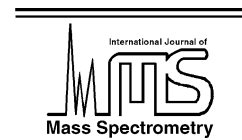




ELSEVIER

International Journal of Mass Spectrometry 222 (2003) 413–430



www.elsevier.com/locate/ijms

Reactions of O_2^+ , NO^+ and H_3O^+ with methylcyclohexane (C_7H_{14}) and cyclooctane (C_8H_{16}) from 298 to 700 K

Anthony J. Midey^{*,1}, Skip Williams, Thomas M. Miller¹, A.A. Viggiano

Air Force Research Laboratory, Space Vehicles Directorate, 29 Randolph Road, Hanscom AFB, MA 01731-3010, USA

Received 10 May 2002; accepted 18 September 2002

Abstract

Rate constants and branching fractions have been measured as a function of temperature for the reactions of O_2^+ , NO^+ and H_3O^+ with methylcyclohexane (C_7H_{14}) and cyclooctane (C_8H_{16}) using fast flow tube methods. The reactions of O_2^+ with both cyclic molecules proceed via non-dissociative and dissociative charge transfer at the capture collision rate from 298 to 700 K. From 298 to 500 K, NO^+ reacts with the two neutral reagents via non-dissociative hydride transfer, and from 500 to 700 K, an increasing fraction of the reaction products are due to dissociative hydride transfer. The rate constants for NO^+ reacting with both C_7H_{14} and C_8H_{16} equal the capture collision rate constants at all temperatures. The H_3O^+ reactions proceed at $\leq 38\%$ and $\leq 22\%$ of the capture collision rate with C_7H_{14} and C_8H_{16} , respectively. The rate constants display a negative temperature dependence with both reagents from 298 to 500 K. Reaction products observed in the H_3O^+ reactions include association, non-dissociative proton transfer and dissociative proton transfer. Increasing amounts of the dissociation products are observed at higher temperatures. (Int J Mass Spectrom 222 (2003) 413–430)

© 2002 Elsevier Science B.V. All rights reserved.

Keywords: Proton transfer; Hydride transfer; Charge transfer; Cycloalkanes; Kinetics; Dissociation

1. Introduction

Cyclic alkanes represent an important class of hydrocarbons and are a significant component of many fuels. For example, the fast igniting and relatively clean burning heavy alkanes found in kerosene or middle distillate fraction petroleum are ideally suited for gas turbine engines used for sub-, trans-, and supersonic propulsion systems. Furthermore, the development of hypersonic propulsion systems (Mach Number > 4) has increased the relative importance of thermal management requirements for fuel selection.

Such requirements have led to the consideration of endothermic fuels that use heat absorbing chemical reactions. For instance, the thermal decomposition reactions of hydrocarbon fuels feature a substantial activation energy barrier, and hence offer a potential heat sink. Moreover, the resulting heat of combustion of the decomposition products remain essentially unchanged or slightly increased. The chemical composition of endothermic fuels has not been precisely defined, but it is apparent that they will comprise saturated linear and cyclic hydrocarbon molecules featuring at least seven carbon atoms. Methylcyclohexane (C_7H_{14}) blends are among the key candidates for such fuels and will pose ignition and flame propagation challenges at hypersonic velocities [1].

* Corresponding author. E-mail: anthony.midey@hanscom.af.mil

¹ Under contract to Visidyne, Inc., Burlington, MA.

The kinetics of ion–molecule chemistry involving hydrocarbon molecules with air plasma ions has been an active topic in recent years [2–16]. One of the primary motivations for the investigations has been to elucidate the role that ions may play in enhancing the combustion of hydrocarbon fuels. Ion–molecule chemistry may be particularly advantageous to issues involving ignition and flame propagation, where high temperature kinetics data are important for accurate computer predictions [17].

However, limited ion–molecule kinetics studies have been done in general, and more specifically, for the two species of interest in this study, methylcyclohexane (C_7H_{14}) and cyclooctane (C_8H_{16}). These two molecules are representative examples of the cycloalkanes as the latter is a large unsubstituted ring structure and the former has a methyl substituent on the ring. One relevant study is that by Spanel et al. [4], where the rate constant and product branching fractions for H_3O^+ reacting with C_7H_{14} was measured at 298 K in a selected ion flow tube (SIFT). The reaction has a rate constant of $7 \times 10^{-10} \text{ cm}^3 \text{ s}^{-1}$, which is less than half of the collision rate constant. Spanel et al. [4] have observed that $C_7H_{13}^+$ is the dominant product ion, and that the proton-transfer product, $C_7H_{15}^+$, is produced in small amounts. These authors have used this kinetic data and known thermodynamic data to estimate the proton affinity of C_7H_{14} to be in the 686–697 kJ mol^{-1} range. This work was motivated by the potential use of chemical ionization mass spectrometers to detect trace neutrals in the atmosphere and in medical applications [2,3,6,18].

In order to further the present level of understanding regarding ions in combustion, in particular ion-enhanced combustion, the ion chemistry of C_7H_{14} and C_8H_{16} has been investigated as a function of temperature for three fundamental classes of ion–molecule reactions, charge transfer, hydride transfer, and proton transfer. Rate constants and branching fractions have been measured for the reactions of O_2^+ and NO^+ with C_7H_{14} and C_8H_{16} from 298 to 700 K with the upper temperature limited by thermal degradation of the neutral reagent. A variable temperature-selected ion flow tube (VT-SIFT) apparatus and high temper-

ature flowing afterglow (HTFA) apparatus have been used in combination to cover the extended temperature range. This approach has been applied successfully with other hydrocarbon species reacting with air plasma ions [11,12,14,16]. Measurements have also been performed on the reaction of H_3O^+ with both cycloalkanes from 298 to 500 K in the VT-SIFT. In some cases, the reaction products observed have not been widely reported and their thermochemical properties are not well characterized in the literature. In these instances, calculations of the geometries and energetics of these species have also been performed and thermochemical properties have been derived. The experimental and computational results are used to rationalize the possible reaction mechanisms involved for each reaction system, including dissociation.

2. Experimental

Two temperature variable flow tube instruments have been used: a VT-SIFT and a HTFA. The instruments are complimentary for the measurement of both thermal rate constants and branching fractions and can be used together to cover temperatures spanning the range of 80–1800 K, although a range of 298–700 K is used in the present studies. Both apparatuses have been described in detail elsewhere [19,20]. Therefore, only the details pertinent to the current results are discussed.

Ions are produced in the VT-SIFT using electron impact on a supersonic expansion [21]. For NO^+ and O_2^+ , electron impact ionization on a supersonic expansion of NO and O_2 with ~ 40 psig backing pressure through a 0.2 mm diameter aperture is employed. These ions are easily generated with a separate effusive source. However, the supersonic source had already been installed and has been used simply for expediency. H_3O^+ is generated by introducing neat room temperature water vapor through a finger inlet into an expansion created using 45 psig Ar behind the nozzle, which is impacted by ca. 50 eV electrons. A complex series of reactions then leads to H_3O^+ . The reactant ions are extracted from the source chamber

and mass selected using a quadrupole mass spectrometer, then injected into a fast flow of He buffer gas from a Venturi inlet.

For the diatomic ions, an additional 3 sccm of NO or 5 sccm of O₂ source gas (<1% of the total gas flow) is introduced at an inlet upstream of the reaction zone to ensure the quenching of both electronically and vibrationally excited reactant ions generated in the source [22]. The cycloalkane reactant is introduced at one of two downstream inlets, and the resulting product and reactant ions are sampled through an aperture in a blunt nose cone. These ions are mass analyzed with a second quadrupole mass filter and detected with a conversion dynode electron multiplier.

The rate constants are determined by measuring the decay of the reactant ion signal over a fixed reaction time as a function of the measured concentration of cycloalkane vapor. For most of the measurements, a flow meter is used to measure the gas flows of the reagents. At 400 and 500 K for the reaction of C₈H₁₆ with H₃O⁺, this method proved inadequate due to a combination of a small rate constant and low vapor pressure of the reactant neutral. Therefore, a measured flow rate of helium carrier gas is bubbled through C₈H₁₆ liquid and the pressure in the vessel is measured to determine the concentration of C₈H₁₆. Unfortunately, the room temperature vapor pressure of C₈H₁₆ has not been reported and the temperature dependence of the vapor pressure around 35 °C is non-linear [23], making an extrapolation using the Clasius–Clapeyron expression unreliable. Therefore, we have measured the vapor pressure of C₈H₁₆ using a capacitance manometer to be 4.8 ± 0.1 Torr at 297 K. This value agrees well with the value of 5.2 Torr extrapolated to 297 K using the Antoine equation for vapor pressure P_{vap} in bars as a function of temperature T (K) as shown in Eq. (1), which has been validated from 370 to 468 K [24]

$$\log_{10}(P_{\text{vap}}) = A - \left(\frac{B}{T + C} \right) \quad (1)$$

where $A = 3.98805$, $B = 1438.687$, and $C = -63.024$.

The experimentally measured vapor pressure has subsequently been used in rate constant measurements

for H₃O⁺ with C₈H₁₆ at 400 and 500 K. The rate constant measurements have relative errors of ±15% and absolute errors of ±25% [20].

The nascent branching fractions are determined by measuring the fractional abundance of each product as a function of the reactant neutral concentration and extrapolating to zero reactant flow. Extrapolating back to zero reactant flow eliminates the effects, if any, arising from secondary chemistry involving the ionic reaction products and neutral reactant. The overall branching fraction of a product channel is measured in two steps: first, the branching between the various C_{*n*} products is measured at low mass resolution to minimize mass discrimination, then the distribution between the C_{*n*}H_{*m*} products separated by one mass unit is measured for a given number of carbons, *n*. A correction is made for the contribution of ¹³C products overlapping with ¹²C products one mass unit higher. The total branching fraction is the product of the low and high mass resolution branching fractions. The errors in the branching fractions are 0.1 times the ratio of a given product fraction to the fraction of the major product ion, plus an additional systematic correction of 0.005 to account for errors in product ions having very low count rates. These limits have been estimated based on considerations of mass discrimination, flow tube diffusion rates, and the total counts of the both reactant and the product ions [8,11].

The HTFA operates in a similar manner as the SIFT. An important difference is that ions produced in a source region perpendicular to the main flow tube are not mass selected before reaction. This source region is a cylindrical canister with several gas inlets that allow source gases to be introduced either before or after a thoriated iridium filament. A detailed description of this new source region and any attendant modifications to the HTFA are given separately [16].

Electron impact on the helium buffer gas entering the source region of the HTFA generates He* which reacts via Penning ionization with either O₂ or NO introduced after the filament to produce O₂⁺ or NO⁺, respectively. A commercial furnace heats an industrial grade quartz flow tube to the desired temperature. The ions and any residual source gas (≤1% of the total

flow) are carried by the buffer gas into the flow tube where thermal equilibration to the flow tube temperature occurs before the reaction region. After reaction occurs for a measured time period over a known distance, the product ions and any remaining reactant ions are sampled through an aperture in a blunt nose cone and mass analyzed with a quadrupole mass filter then detected.

The reagents used in the experiments are as follows. Water vapor is removed from the He buffer gas (99.997%) by passing it through a liquid nitrogen-cooled sieve trap. The liquid C₈H₁₆ (Aldrich, 99+%) and C₇H₁₄ (Aldrich, 99%) samples have been used as obtained without further purification, aside from several freeze–pump–thaw cycles performed to remove trapped gases. The distilled water used in the ion source of the VT-SIFT for the H₃O⁺ experiments has been cleared of trapped gases by pumping.

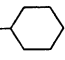
3. Results

The results for the reactions of O₂⁺, NO⁺ and H₃O⁺ with C₇H₁₄ and C₈H₁₆ are listed in Tables 1–6. The VT-SIFT and HTFA data are shown together in Tables 1–4 for the O₂⁺ and NO⁺ reactions. The enthalpy of reaction at 298 K and the average total reaction energy at each temperature are also listed in Tables 1–6, where the average energy available for reaction at temperature *T* is given by Eq. (2)

$$\langle E_{\text{rxn}}(T) \rangle = \langle \text{KE} \rangle + \langle E_{\text{int}}^{\text{ion}} \rangle + \langle E_{\text{vib}}^{\text{neut}} \rangle + \langle E_{\text{rot}}^{\text{neut}} \rangle \quad (2)$$

The average center-of-mass kinetic energy $\langle \text{KE} \rangle$ is $(3/2)k_{\text{B}}T$ while the average internal energy of the ion $\langle E_{\text{int}}^{\text{ion}} \rangle$ is the sum of the average rotational and vibrational energy. The diatomic ions have an average rotational energy of $k_{\text{B}}T$ and H₃O⁺ has an average

Table 1
Rate constants and branching fractions for the reaction of O₂⁺ with C₇H₁₄ in the VT-SIFT and the HTFA from 298 to 700 K

O ₂ ⁺ + C ₇ H ₁₄ →	Methylcyclohexane H ₃ C 	$\Delta H_{\text{rxn}}^{298}$ (kJ mol ⁻¹)	Rate constant, [<i>k_c</i>] (×10 ⁻⁹ cm ³ s ⁻¹) branching fraction				
			SIFT (298 K)	SIFT (400 K)	SIFT (500 K)	HTFA (500 K)	HTFA (700 K)
			$\langle E_{\text{rxn}} \rangle$ (kJ mol ⁻¹)				
			22	38	58	58	111
	Products		1.8 [1.7]	1.7 [1.7]	1.9 [1.7]	1.7 [1.7]	1.6 [1.7]
	c-C ₇ H ₁₄ ⁺ + O ₂	-233	0.42	0.30	0.10	0.06	0.01
	(c-C ₇ H ₁₃ ⁺ + H + O ₂)	-132 ^{a,b}	0.01	0.01		0.02	
	(c-C ₆ H ₁₁ ⁺ + CH ₃ + O ₂)	-132	0.36	0.42	0.58	0.56	0.48
	(c-C ₆ H ₁₀ ⁺ + CH ₄ + O ₂)	-227	0.08	0.08	0.12	0.18	0.15
	(<i>t</i> -C ₅ H ₁₀ ⁺ + C ₂ H ₄ + O ₂)	-163	0.04	0.04	0.06	0.04	0.07
	(<i>t</i> -C ₅ H ₉ ⁺ + C ₂ H ₅ + O ₂)	-126	0.03	0.04	0.04	0.04	0.07
	(<i>t</i> -C ₅ H ₈ ⁺ + C ₂ H ₆ + O ₂)	-167	0.02	0.03	0.02	0.04	0.07
	(<i>s</i> -C ₅ H ₇ ⁺ + C ₂ H ₆ + H + O ₂)	45					0.01
	(<i>t</i> -C ₄ H ₉ ⁺ + C ₃ H ₅ + O ₂)	-146		0.01	0.01	0.01	0.01
	(<i>s</i> -C ₄ H ₈ ⁺ + C ₃ H ₆ + O ₂)	-124	0.03	0.05	0.05	0.04	0.08
	(<i>s</i> -C ₄ H ₇ ⁺ + C ₃ H ₇ + O ₂)	-75	0.01	0.02	0.02		0.01
	(C ₄ H ₆ ⁺ + C ₃ H ₈ + O ₂)	96					0.01
	(<i>t</i> -C ₃ H ₇ ⁺ + C ₄ H ₇ + O ₂)	-79			0.01	<0.01	0.01
	(<i>s</i> -C ₃ H ₆ ⁺ + C ₄ H ₈ + O ₂)	-64				<0.01	0.01


The collision rate constants, *k_c*, are given in brackets, along with the experimental values, both of which have units of 10⁻⁹ cm³ s⁻¹. The standard reaction enthalpies at 298 K and the average total reaction energy available at each temperature are both given in units of kJ mol⁻¹. Unless otherwise noted with a c for cyclic, all of the structures are assumed to be non-cyclic. s, secondary cation; t, tertiary cation.

^a Calculated from theory. See text for details.

^b H₃C-c-C₆H₁₀⁺.

Table 2

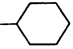
Rate constants and branching fractions for the reaction of O₂⁺ with C₈H₁₆ in the VT-SIFT and the HTFA from 298 to 700 K as in Table 1

Cyclooctane 	$\Delta H_{\text{rxn}}^{298}$ (kJ mol ⁻¹)	Rate constant [<i>k_c</i>] (×10 ⁻⁹ cm ³ s ⁻¹) branching fraction				
		SIFT (298 K)	SIFT (400 K)	SIFT (500 K)	HTFA (500 K)	HTFA (700 K)
		$\langle E_{\text{rxn}} \rangle$ (kJ mol ⁻¹)				
		25	43	66	66	126
O ₂ ⁺ + C ₈ H ₁₆ →	Products	1.7 [1.8]	1.8 [1.8]	1.9 [1.8]	2.0 [1.8]	2.1 [1.8]
	c-C ₈ H ₁₆ ⁺ + O ₂	0.31	0.16	0.02	0.01	
	c-C ₈ H ₁₅ ⁺ + H + O ₂	0.02	0.01	0.01	0.01	
	(<i>t</i> -C ₇ H ₁₃ ⁺ + CH ₃ + O ₂)	0.03	0.04	0.04	0.05	0.04
	(<i>s</i> -C ₆ H ₁₂ ⁺ + C ₂ H ₄ + O ₂)	0.13	0.15	0.16	0.09	0.06
	(<i>t</i> -C ₆ H ₁₁ ⁺ + C ₂ H ₅ + O ₂)	0.13	0.15	0.18	0.18	0.18
	(<i>s</i> -C ₆ H ₁₀ ⁺ + C ₂ H ₆ + O ₂)	0.03	0.04	0.05	0.07	0.02
	(<i>s</i> -C ₅ H ₁₁ ⁺ + C ₃ H ₅ + O ₂)	0.01	0.01	0.02		
	(<i>s</i> -C ₅ H ₁₀ ⁺ + C ₃ H ₆ + O ₂)	0.12	0.16	0.19	0.15	0.17
	(<i>s</i> -C ₅ H ₉ ⁺ + C ₃ H ₇ + O ₂)	0.05	0.05	0.07	0.09	0.13
	(<i>s</i> -C ₅ H ₈ ⁺ + C ₃ H ₈ + O ₂)	0.04	0.05	0.04	0.09	0.06
	(<i>s</i> -C ₅ H ₇ ⁺ + C ₃ H ₈ + H + O ₂)				0.02	0.04
	(<i>s</i> -C ₄ H ₉ ⁺ + C ₄ H ₇ + O ₂)	0.02	0.02	0.03	0.03	0.03
	(<i>s</i> -C ₄ H ₈ ⁺ + C ₄ H ₈ + O ₂)	0.08	0.11	0.13	0.15	0.02
	(<i>s</i> -C ₄ H ₇ ⁺ + C ₄ H ₉ + O ₂)	0.01	0.01	0.02	0.03	0.17
	(<i>s</i> -C ₄ H ₆ ⁺ + C ₄ H ₁₀ + O ₂)				0.01	0.01
	(<i>t</i> -C ₃ H ₇ ⁺ + C ₅ H ₉ + O ₂)		0.02	0.04	0.02	0.02
	(<i>s</i> -C ₃ H ₆ ⁺ + C ₅ H ₁₀ + O ₂)		0.01		0.02	0.02

s, secondary cation; *t*, tertiary cation.^a Calculated from theory. See text for details.

Table 3

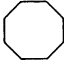
Rate constants and branching fractions for the reaction of NO⁺ with C₇H₁₄ in the VT-SIFT and the HTFA from 298 to 700 K as in Table 1

Methylcyclohexane 	$\Delta H_{\text{rxn}}^{298}$ (kJ mol ⁻¹)	Rate constant [<i>k_c</i>] (×10 ⁻⁹ cm ³ s ⁻¹) branching fraction				
		SIFT (298 K)	SIFT (400 K)	SIFT (500 K)	HTFA (500 K)	HTFA (700 K)
		$\langle E_{\text{rxn}} \rangle$ (kJ mol ⁻¹)				
		22	38	58	58	111
NO ⁺ + C ₇ H ₁₄ →	Products	1.9 [1.8]	1.8 [1.8]	1.6 [1.8]	1.9 [1.8]	1.8 [1.8]
	c-C ₇ H ₁₄ ⁺ + NO		39	0.01	0.01	<0.01
	(c-C ₇ H ₁₃ ⁺ + HNO)	1.00	-55 ^{a,b}	0.98	0.99	0.89
	(<i>t</i> -C ₅ H ₉ ⁺ + C ₂ H ₄ + HNO)		77			0.02
	(<i>s</i> -C ₄ H ₈ ⁺ + C ₃ H ₆ + NO)		148	0.01		<0.01
	(<i>s</i> -C ₄ H ₇ ⁺ + C ₃ H ₆ + HNO)		135	0.01	0.01	0.08

s, secondary cation; *t*, tertiary cation.^a Calculated from theory. See text for details.^b H₃C-c-C₆H₁₀⁺.

Table 4

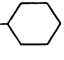
Rate constants and branching fractions for the reaction of NO⁺ with C₈H₁₆ in the VT-SIFT and the HTFA from 298 to 700 K as in Table 1

Cyclooctane 	$\Delta H_{\text{rxn}}^{298}$ (kJ mol ⁻¹)	Rate constant [k_c] ($\times 10^{-9}$ cm ³ s ⁻¹) branching fraction					
		SIFT (298 K)	SIFT (400 K)	SIFT (500 K)	HTFA (500 K)	HTFA (600 K)	HTFA (700 K)
		$\langle E_{\text{rxn}} \rangle$ (kJ mol ⁻¹)					
		25	43	66	66	94	126
NO ⁺ + C ₈ H ₁₆ →	Products	1.9 [1.9]	1.7 [1.9]	1.7 [1.9]	2.1 [1.9]	1.9 [1.9]	1.9 [1.9]
	c-C ₈ H ₁₆ ⁺ + NO		0.02	0.02	0.05	0.05	
	c-C ₈ H ₁₅ ⁺ + HNO	0.99	0.97	0.95	0.95	0.67	0.15
	(<i>t</i> -C ₇ H ₁₃ ⁺ + CH ₃ + NO)	0.01					0.01
	(<i>t</i> -C ₆ H ₁₁ ⁺ + C ₂ H ₄ + HNO)						0.01
	(<i>s</i> -C ₅ H ₉ ⁺ + C ₃ H ₆ + HNO)			0.02		0.28	0.81
	(<i>s</i> -C ₄ H ₉ ⁺ + C ₄ H ₇ + NO)						0.01
	(<i>s</i> -C ₄ H ₈ ⁺ + C ₄ H ₈ + NO)		<0.01	<0.01			
	(<i>s</i> -C ₄ H ₇ ⁺ + C ₄ H ₈ + HNO)		<0.01	<0.01			0.01

s, secondary cation; *t*, tertiary cation.^a Calculated from theory. See text for details.

Table 5

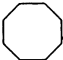
Rate constants and branching fractions for the reaction of H₃O⁺ with C₇H₁₄ in the VT-SIFT from 298 to 700 K as in Table 1

Methylcyclohexane 	$\Delta H_{\text{rxn}}^{298}$ (kJ mol ⁻¹)	Rate constant [k_c] ($\times 10^{-9}$ cm ³ s ⁻¹) branching fraction		
		SIFT (298 K)	SIFT (400 K)	SIFT (500 K)
		$\langle E_{\text{rxn}} \rangle$ (kJ mol ⁻¹)		
		23	40	61
H ₃ O ⁺ + C ₇ H ₁₄ →	Products	0.8 [2.1]	0.6 [2.1]	0.4 [2.1]
	H ₃ O ⁺ (C ₇ H ₁₄)	0.01		
	(<i>t</i> -C ₇ H ₁₅ ⁺ + H ₂ O)	0.05	0.08	0.01
	(c-C ₇ H ₁₄ ⁺ + H + H ₂ O)	318	0.01	
	(c-C ₇ H ₁₃ ⁺ + H ₂ + H ₂ O)	0.88	0.75	0.68
	(c-C ₆ H ₁₁ ⁺ + CH ₄ + H ₂ O)	0.06	0.07	0.10
	(<i>s</i> -C ₅ H ₁₀ ⁺ + C ₂ H ₅ + H ₂ O)	280	0.01	0.03
	(<i>t</i> -C ₅ H ₉ ⁺ + C ₂ H ₆ + H ₂ O)	5	0.01	0.01
	(<i>t</i> -C ₅ H ₈ ⁺ + C ₂ H ₆ + H + H ₂ O)	384	0.01	0.01
	(C ₄ H ₁₀ ⁺ + C ₃ H ₅ + H ₂ O)	382	0.01	
	(<i>t</i> -C ₄ H ₉ ⁺ + C ₃ H ₆ + H ₂ O)	36	0.04	0.11
	(<i>s</i> -C ₄ H ₈ ⁺ + C ₃ H ₇ + H ₂ O)	278		0.02
	(<i>s</i> -C ₄ H ₇ ⁺ + C ₃ H ₈ + H ₂ O)	62		0.02

s, secondary cation; *t*, tertiary cation.^a Calculated from theory. See text for details.^b H₃C-c-C₆H₁₀⁺.

Table 6

Rate constants and branching fractions for the reaction of H_3O^+ with C_8H_{16} in the VT-SIFT and the HTFA from 298 to 700 K as in Table 1

	Cyclooctane 	$\Delta H_{\text{rxn}}^{298}$ (kJ mol ⁻¹)	Rate constant [k_c] ($\times 10^{-9}$ cm ³ s ⁻¹) branching fraction		
			SIFT (298 K)	SIFT (400 K)	SIFT (500 K)
			$\langle E_{\text{rxn}} \rangle$ (kJ mol ⁻¹)		
			26	45	69
$\text{H}_3\text{O}^+ + \text{C}_8\text{H}_{16} \rightarrow$	Products		0.5 [2.3]	0.3 [2.3]	0.3 [2.3]
	$\text{H}_3\text{O}^+(\text{C}_8\text{H}_{16})$		0.30		
	(<i>s</i> - $\text{C}_8\text{H}_{17}^+ + \text{H}_2\text{O}$)	-63	0.45	0.20	
	(<i>c</i> - $\text{C}_8\text{H}_{15}^+ + \text{H}_2 + \text{H}_2\text{O}$)	-74 ^a	0.06	0.10	0.15
	(<i>s</i> - $\text{C}_6\text{H}_{12}^+ + \text{C}_2\text{H}_5 + \text{H}_2\text{O}$)	224		0.01	0.03
	(<i>s</i> - $\text{C}_6\text{H}_{11}^+ + \text{C}_2\text{H}_6 + \text{H}_2\text{O}$)	-86		0.02	0.03
	(<i>s</i> - $\text{C}_5\text{H}_{11}^+ + \text{C}_3\text{H}_6 + \text{H}_2\text{O}$)	44	0.16	0.35	0.34
	(<i>s</i> - $\text{C}_5\text{H}_{10}^+ + \text{C}_3\text{H}_7 + \text{H}_2\text{O}$)	232			0.04
	(<i>s</i> - $\text{C}_5\text{H}_9^+ + \text{C}_3\text{H}_8 + \text{H}_2\text{O}$)	-50	0.03	0.05	0.06
	(<i>s</i> - $\text{C}_4\text{H}_9^+ + \text{C}_4\text{H}_8 + \text{H}_2\text{O}$)	45		0.16	0.25
	(<i>s</i> - $\text{C}_4\text{H}_8^+ + \text{C}_4\text{H}_9 + \text{H}_2\text{O}$)	231		0.07	0.05
	(<i>s</i> - $\text{C}_4\text{H}_7^+ + \text{C}_4\text{H}_{10} + \text{H}_2\text{O}$)	11		0.04	0.05

s, secondary cation; *t*, tertiary cation.^a Calculated from theory. See text for details.

rotational energy equal to $(3/2)k_{\text{B}}T$. The average rotational energy of the neutral reactants, $\langle E_{\text{rot}}^{\text{neut}} \rangle$, is $(3/2)k_{\text{B}}T$ for both cycloalkanes. $\langle E_{\text{vib}}^{\text{neut}} \rangle$ is the average vibrational energy of the neutral reactant and is discussed in the following sections.

The average vibrational energy is an ensemble average over a Boltzmann distribution of vibrational energy levels for the $3N-6$ modes in the harmonic approximation, neglecting zero-point energy (ZPE). The vibrational energy contribution of NO^+ and O_2^+ is relatively small at all temperatures because excited vibrational levels are not significantly populated due to the high frequency of vibration. However, the vibrational energy contribution for H_3O^+ and the cycloalkanes can be significant over the temperature range studied. Vibrational frequencies for H_3O^+ have been taken from the NIST-JANNAF Tables [25]. The frequencies for C_7H_{14} and C_8H_{16} have been calculated using *Gaussian 98W* at the Hartree–Fock (HF)/6-31G(*d*) level for geometry optimized structures [26].

The reaction enthalpies at 298 K in Tables 1–6 have been calculated from the compiled literature values of

Lias et al. [24,27] unless otherwise noted. Notable exceptions are the reaction enthalpies for proton transfer and hydride transfer where theoretical calculations have been conducted as discussed in the following sections. The calculations have been required because literature thermochemical values are non-existent to calculate the enthalpy of reaction for forming $\text{C}_8\text{H}_{15}^+$ and $\text{C}_8\text{H}_{17}^+$ from C_8H_{16} with the C_8 ring structure unbroken. However, estimated thermochemical data are available to calculate the enthalpy of reaction for forming $\text{C}_7\text{H}_{13}^+$ [27] and $\text{C}_7\text{H}_{15}^+$ [4] from C_7H_{14} with the cyclohexane ring intact, and these values are used as a basis for comparison with the theoretical calculations performed as part of this study.

The thermal stability of the neutral parent hydrocarbon limits the maximum temperature reported. One indication of pyrolysis of the parent hydrocarbon (i.e., thermal decomposition) is the appearance of numerous hydrogen-depleted ions not observed at lower temperatures as noted in our previous study [14]. Thermal decomposition data for the C_7H_{14} and C_8H_{16} reactants under our experimental conditions, i.e., 1 Torr of He pressure and millisecond

residence times, is not available to our knowledge. However, hydrogen depletion is a good indication of decomposition because hydrogen elimination is typically the most energetically favorable pathway and is often the first observed in the pyrolysis of hydrocarbons [28]. The data in Tables 3 and 4 listing the reaction products for the reactions of NO^+ with C_7H_{14} and C_8H_{16} , respectively, indicate that these cyclic hydrocarbons are stable under our conditions. If the reactants had partially decomposed, ions other than those listed would be formed from NO^+ hydride transfer reactions with the hydrogen-depleted pyrolysis products of the starting cycloalkanes. Based on the branching fractions listed in Tables 3 and 4, less than 3% of the total reactivity of C_7H_{14} and less than 4% of the total reactivity of C_8H_{16} are attributed to reaction with the pyrolysis products of the reactant cycloalkane up to 700 K.

The chemical pathways leading to the formation of the major product ions shown in the figures and listed in the tables are discussed in the following sections. The minor product channels, on the order of 0.01–0.04 branching fraction, observed at high temperature are not discussed in detail, because these products cannot conclusively be distinguished from reactions with the primary ions and any trace pyrolysis byproducts present in the flow tube. However, these product channels are listed for completeness in Tables 1–6. Furthermore, several products are shown in parentheses reflecting the uncertainty in the neutral products, which are not directly observed in our experiments. In most cases, the most energetically favorable, mechanistically feasible pathway is listed. For all of the species listed, the most stable isomeric form is assumed, i.e., the isomer with the lowest standard heat of formation.

3.1. Theoretical calculations

The 298 K reaction enthalpies have been calculated using Gaussian 98W [26] for the reactions of NO^+ with C_7H_{14} and C_8H_{16} to form $\text{C}_7\text{H}_{13}^+$ and $\text{C}_8\text{H}_{15}^+$, respectively, H_3O^+ with C_7H_{14} to form $\text{C}_7\text{H}_{15}^+$ and $\text{C}_7\text{H}_{13}^+$ and H_3O^+ with C_8H_{16} to form $\text{C}_8\text{H}_{17}^+$ and

$\text{C}_8\text{H}_{15}^+$. The standard reaction enthalpies have been determined by optimizing the geometry of all species involved in the reaction at the same level of theory and performing higher level single point energy calculations [29].

The highest level of theory that is computationally cost effective has been utilized. Both the lowest energy structures and final optimized geometries are calculated initially using the HF method at the 6-31G(d) level. For $\text{C}_7\text{H}_{13}^+$ and $\text{C}_8\text{H}_{15}^+$, an H^- has been removed from each carbon and the ion geometry subsequently optimized for each individual ionic structure. The lowest energy structure at this level of theory has then been used as a starting point for the higher level calculations. A similar set of optimizations has been done for $\text{C}_7\text{H}_{15}^+$ and $\text{C}_8\text{H}_{17}^+$ with an H^+ placed on each carbon atom.

The stability of all of the lower level geometries has been confirmed prior to using them as the starting point for the higher level calculations. For C_7H_{14} , the thermochemistry has been determined using the G2(MP2) method [30]. However, density functional theory (DFT) has been used at the B3LYP level with the 6-311++G(3df, 2p) basis set for the larger C_8H_{16} molecule for both the geometry optimization and frequency calculations used to determine the relevant thermochemical quantities.

The G2(MP2) calculations automatically include scaling corrections to the theoretical frequencies that remove basis set-dependent systematic errors that will be reflected in the ZPE and thermal corrections to the enthalpy. For the G2(MP2) method, this correction is 0.8929. Bauschlicher and Partridge have shown by comparison with experimentally determined ZPE's that the average scaling factor for B3LYP using the 6-311++G(3df, 2p) basis set is 0.989, giving average errors in the ZPE of 0.2 kJ mol^{-1} and maximum errors of 1.05 kJ mol^{-1} [31]. This error is an insignificant contribution to the uncertainty in the reaction enthalpies. Thus, similar scaling has not been applied in the present DFT results. The mean absolute deviation from experimental values of the G2(MP2) theory [30] is 6.61 kJ mol^{-1} and of the B3LYP/6-311++G(3df, 2p) theory [31] is 9.29 kJ mol^{-1} . To allow for any

additional errors not accounted for beyond the average errors above, the thermochemical values calculated presently from theory have reported errors of $\pm 7 \text{ kJ mol}^{-1}$ for C_7H_{14} and $\pm 10 \text{ kJ mol}^{-1}$ for C_8H_{16} .

3.2. O_2^+ reactions

For both cycloalkanes, reaction with O_2^+ occurs at the Su-Chesnavich collision rate [32,33] over the entire temperature range. Fig. 1a (C_7H_{14}) and 1b (C_8H_{16}) show the C_mH_n branching fractions as a function of temperature for $n = 3-7$ and $n = 3-8$, respectively. In Fig. 1, all species with the same number of carbon atoms but differing by some number of H atoms are grouped together. The individual product channel branching fractions, reaction enthalpies and

average energies available for reaction are given in Tables 1 and 2, respectively. The non-dissociative charge-transfer channel is highly exothermic for both reactions and is the most abundant product in both reactions at room temperature. However, many dissociative charge-transfer channels are also exothermic and ring-breaking products are observed at all temperatures. An increasing amount of fragmentation is observed as the temperature increases, which is consistent with more energy being available for dissociation. No appreciable non-dissociative charge-transfer product ion signal is observed at 700 K for both cyclic reagents. The reactions occur via non-dissociative and dissociative charge-transfer at all temperatures, and the neutral reaction products listed in Tables 1 and 2 reflect this assumption.

Figs. 2 and 3 illustrate the temperature dependences of the individual fragment channels for the O_2^+ reactions with C_7H_{14} and C_8H_{16} , respectively. The SIFT data are given by the solid symbols and the HTFA data are given by the open symbols. The most prevalent dissociation products are those associated with stable straight chain alkane or alkene neutral fragments, particularly C_2H_4 , C_3H_6 , and C_4H_8 . The C_6 products from C_7H_{14} are assumed to have the cyclohexane ring intact because these cyclic ions are the most stable and mechanistically easiest to produce as they primarily involve removal of the methyl substituent. For C_8H_{16} , on the other hand, the C_7 and C_6 product ions could be non-cyclic as the octagonal structure must be destroyed for carbon loss to occur. The $\text{C}_7\text{H}_{13}^+$ observed in the C_8H_{16} reaction is presumably not the tertiary carbocation structure with a cyclohexane ring described for the C_7H_{14} reaction. Such a process would involve breaking the 8-membered ring structure and reforming a 6-membered ring structure. Therefore, a non-cyclic structure for $\text{C}_7\text{H}_{13}^+$ has been assumed in order to calculate the reaction enthalpy in Table 2.

Many different isomers exist for the potential C_4 – C_7 product ions and neutrals and all are energetically possible with both C_8H_{16} and C_7H_{14} . Furthermore, all of the probable structures involve hydrogen migration and rearrangements to a certain degree, precluding a mechanistic advantage to one species. Therefore, it is

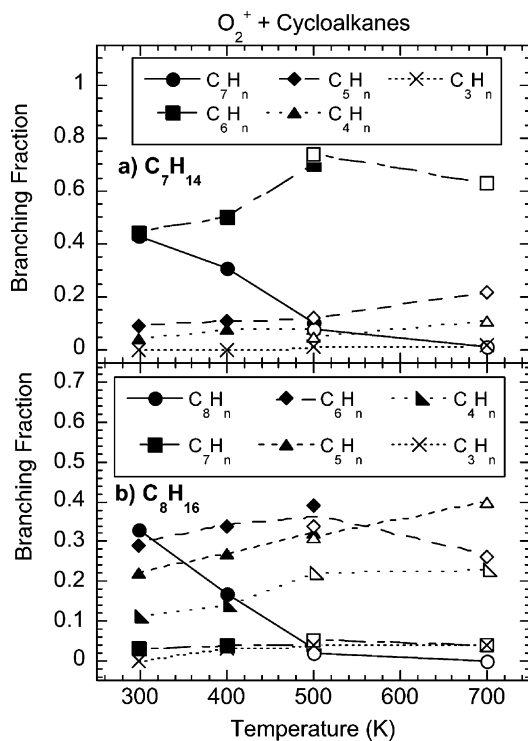


Fig. 1. (a) C_mH_n branching fractions where $m = 3-7$ for O_2^+ reaction with C_7H_{14} vs. temperature in K. (b) C_mH_n branching fractions where $m = 3-7$ for O_2^+ reaction with C_8H_{16} vs. temperature in K. In both plots, the open symbols have been measured in the VT-SIFT and the solid symbols have been measured in the HTFA. The lines are shown as a guide to the eye.

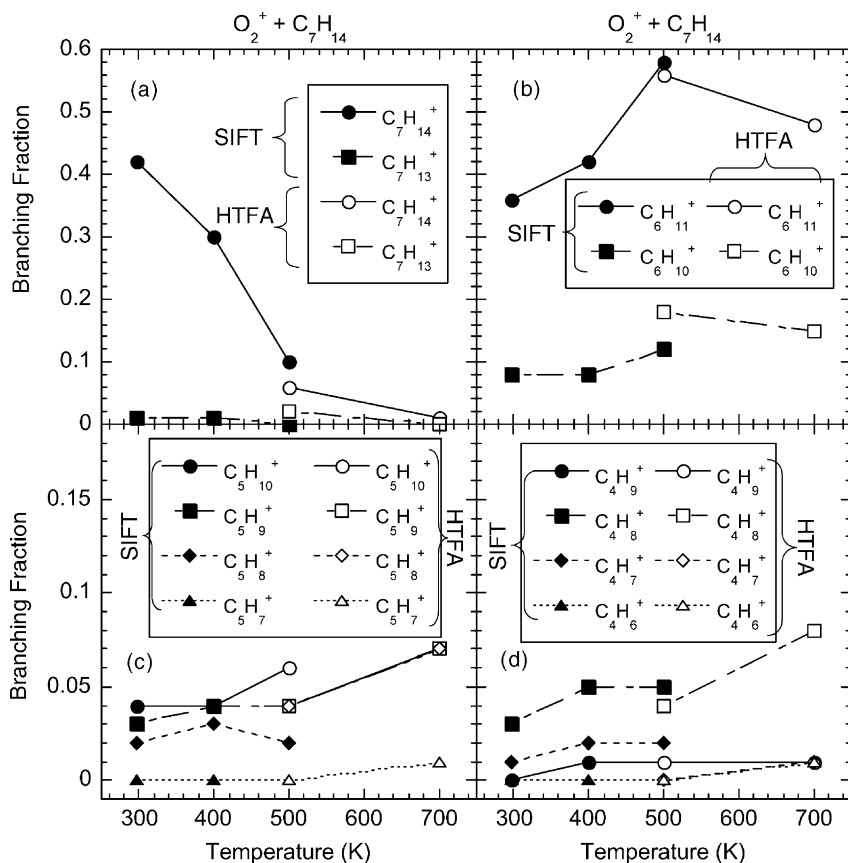


Fig. 2. (a) C_7H_n branching fractions. (b) C_6H_n branching fractions. (c) C_5H_n branching fractions. (d) C_4H_n branching fractions for the reaction of O_2^+ with C_7H_{14} vs. temperature in K. In all plots, the open symbols have been measured in the VT-SIFT and the solid symbols have been measured in the HTFA. The lines are shown as a guide to the eye.

difficult to assign a final structure based only on the energetics for the O_2^+ reaction. Consequently, the reaction enthalpies given in Tables 1 and 2 have been calculated using the lowest energy non-cyclic species [24,27], unless that structure would require significant rearrangement, in particular, extended or multiple carbon migration.

Examining Figs. 1–3 and Tables 1 and 2 shows that the HTFA and VT-SIFT data agree well within the noted experimental errors consistent with our previous experiments utilizing a combination of the two instruments [11,12,14,16]. The low-resolution branching fractions at 500 K in the HTFA for C_8H_{16} appear to be skewed more toward the C_5 products vs. the C_6 products compared to the results obtained in the

SIFT. In addition, the high-resolution branching fractions show minor discrepancies for the $C_7H_{14}^+$ and $C_6H_{10}^+$ channels with C_7H_{14} and $C_6H_{12}^+$, $C_5H_{10}^+$ and $C_5H_8^+$ channels with C_8H_{16} . The HTFA product fractions tend toward larger amounts of the smaller fragment ions.

One obvious source of the minor discrepancies may be varying reaction conditions between the two instruments. For instance, in the HTFA the source region is not isolated as it is in the VT-SIFT. In order to check for possible systematic differences, the branching ratios were measured as a function of O_2 source gas flow, nose cone sampling voltage, electron impact filament emission current, and focusing conditions in the sampling region in the HTFA. Sampling conditions and

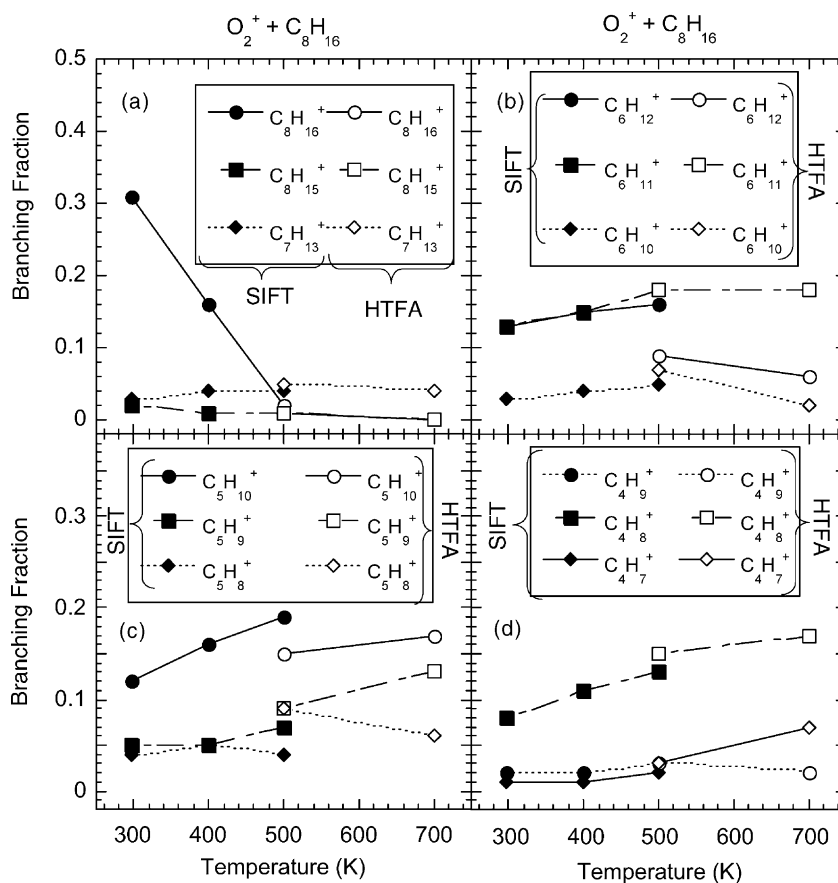


Fig. 3. (a) C_8H_n and C_7H_n branching fractions. (b) C_6H_n branching fractions. (c) C_5H_n branching fractions. (d) C_4H_n branching fractions for the reaction of O_2^+ with C_7H_{14} vs. temperature in K. In all plots, the open symbols have been measured in the VT-SIFT and the solid symbols have been measured in the HTFA. The lines are shown as a guide to the eye.

flow tube pressure in the VT-SIFT were also varied. The branching fractions observed did not change systematically as a function of these conditions. Typical variations are a few percent, which is within the expected variation of the measurements. The presence of impurity ions in the flow tube and O^+ ions from incomplete source chemistry have also been considered, but these ions were found to account for $\leq 1\%$ of the total reactant ions present.

Previous flow tube experiments at high temperatures have shown that ring-breaking reactions can occur through dissociation of a long-lived charge-transfer product ion in collisions with the helium bath gas. The non-dissociative charge-transfer ions can persist for

long times (>1 ms) despite storing large amounts of vibrational energy. The long-lifetimes of the nascent product ions allow multiple collisions with the bath gas to occur [14]. If the small discrepancies noted above result from collisionally activated unimolecular dissociation of the parent ion, variations in pressure should change the branching fractions. The operating pressures used in the HTFA are typically 1 Torr compared to ca. 0.5 Torr in the VT-SIFT. Consequently, the increased pressure of the HTFA would lead to more dissociation. To confirm this hypothesis, pressure variations over a ca. 0.3 Torr range were produced in the VT-SIFT. However, this limited variation yielded no measurable dependence. Therefore, while

collisionally activated unimolecular dissociation may be responsible for the small variation in the branching fractions between the two instruments, it could not be confirmed based on the limited variability in the pressure that could be explored.

Computationally, the reaction of O_2^+ with C_7H_{14} to form $C_7H_{13}^+$ is used to validate the theoretical approach adopted to determine unavailable thermochemical values and has a theoretically calculated reaction enthalpy at 298 K of $-132 \pm 7 \text{ kJ mol}^{-1}$ as shown in Table 1. The calculations have been performed assuming that the hydrogen atom has been removed from the ring carbon that has the methyl group attached to it. The resulting ion is a tertiary carbocation and is the most stable cation. The reaction enthalpy is found to be $-138 \pm 8 \text{ kJ mol}^{-1}$ using the heat of formation for $C_7H_{13}^+$ estimated by Lias et al. [27] from the proton affinity of methylcyclohexene (C_7H_{12}). This agrees with the theoretical value within the estimated error of the calculation.

3.3. NO^+ reactions

Hydride transfer to NO^+ , forming HNO, is exothermic at 298 K for both C_7H_{14} and C_8H_{16} . Both reactions proceed at the Su-Chesnavich collision rate within the experimental error at all temperatures [32,33]. Examining Table 3, non-dissociative hydride transfer is observed as the dominant channel for the reaction of NO^+ with C_7H_{14} . However, approximately 10% dissociation occurs at 700 K, where the total reaction energy is highest. The most abundant dissociative product ion from C_7H_{14} is $C_4H_7^+$ at 700 K. In the reaction of NO^+ with C_8H_{16} at temperatures of 600 K or lower, non-dissociative hydride transfer is also the dominant channel. At 700 K, dissociative hydride transfer forming $C_5H_9^+$ becomes the dominant channel as seen in Table 4. Note that in both reactions the dominant neutral products for the dissociative hydride transfer are C_3H_6 plus HNO.

The trends in the primary product distributions with temperature are shown in Fig. 4a (C_7H_{14}) and 4b (C_8H_{16}). The HTFA and VT-SIFT data agree very well. The branching fractions for C_8H_{16} show a steep

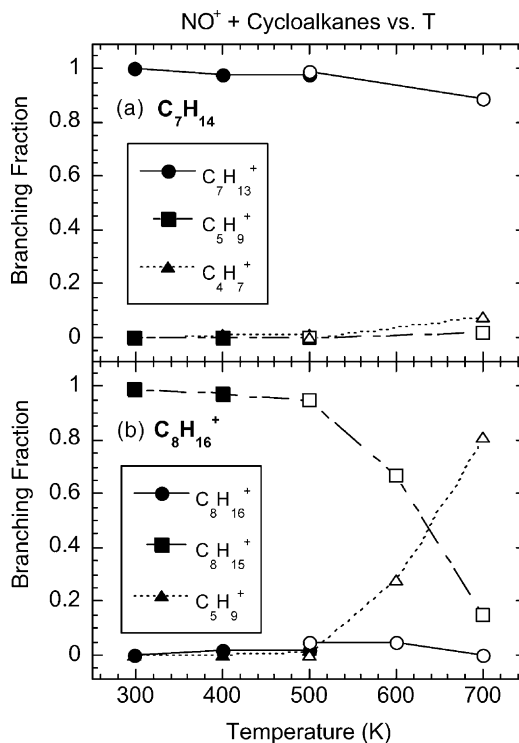


Fig. 4. (a) C_mH_n branching fractions where $m = 4-7$ for NO^+ reaction with C_7H_{14} vs. temperature in K. (b) C_mH_n branching fractions where $m = 4-7$ for NO^+ reaction with C_8H_{16} vs. temperature in K. In both plots, the open symbols have been measured in the VT-SIFT and the solid symbols have been measured in the HTFA. The lines are shown as a guide to the eye.

temperature dependence with an onset for dissociation around 500 K. The dissociative channel is endothermic by 23 kJ mol^{-1} . However, the available energy is more than sufficient to overcome the reaction endothermicity, even at room temperature. For C_7H_{14} , dissociation is more endothermic and only starts to become important when the energy available for reaction approaches the endothermicity.

3.4. H_3O^+ reactions

The reactions of H_3O^+ with C_7H_{14} and C_8H_{16} are intriguing. The rate constants are less than the Su-Chesnavich collision rate [32,33], despite the fact that the reactions are exothermic. The reaction enthalpies for $C_7H_{15}^+$ and $C_8H_{17}^+$ formation shown

in Tables 5 and 6 have been determined assuming a linear structure based on the results of theoretical calculations showing that the minimum energy structures for both protonated cycloalkanes do not favor a cyclic structure with a proton attached. For non-cyclic $C_7H_{15}^+$, a tertiary carbocation can easily be formed which is the lowest energy non-cyclic structure not requiring carbon migration [27]. For the reaction with C_8H_{16} , the estimated heat of formation of Arnold et al. [9] for a linear $C_8H_{17}^+$ secondary carbocation formed via proton transfer from H_3O^+ to *n*-octane (C_8H_{18}) is used. The validity of a linear structure assumption will be examined in Section 4.

Fig. 5a and b show the branching fractions as a function of temperature for C_7H_{14} and C_8H_{16} , respectively. For C_7H_{14} , a small amount of an association product is observed at room temperature (1%) and non-dissociative proton transfer is observed at all temperatures. The main product channel observed at all temperatures with C_7H_{14} is proton transfer followed by H_2 elimination, giving $C_7H_{13}^+$. Assuming the same tertiary carbocation structure forms as in the O_2^+ and NO^+ reactions with C_7H_{14} , the theoretically computed reaction enthalpy at 298 K is -28 kJ mol^{-1} . This value compares well with the value of -23 kJ mol^{-1} obtained using the Lias et al. [27] enthalpy of formation for $C_7H_{13}^+$ discussed previously. Another appreciable channel (6–10%) at all temperatures is $C_6H_{11}^+$. This ion most likely results from proton transfer followed by CH_4 loss that leaves the cyclohexane ring intact. At high temperatures, the second most abundant channel is $C_4H_9^+$, which is proton transfer followed by C_3H_6 elimination. The tertiary butyl ion is the most stable $C_4H_9^+$ isomeric structure and mechanistically easiest if this fragment comes from the methyl substituted end of the ring. Spanel et al. [4] have found that 95% of the products observed with C_7H_{14} at 298 K result in $C_7H_{13}^+$ with an H_2 fragment, with the rest of the products being $C_7H_{15}^+$. Their branching fractions are in general agreement with the current results that show almost 90% $C_7H_{13}^+$.

For H_3O^+ reacting with C_8H_{16} , non-dissociative proton transfer is the main product at room temper-

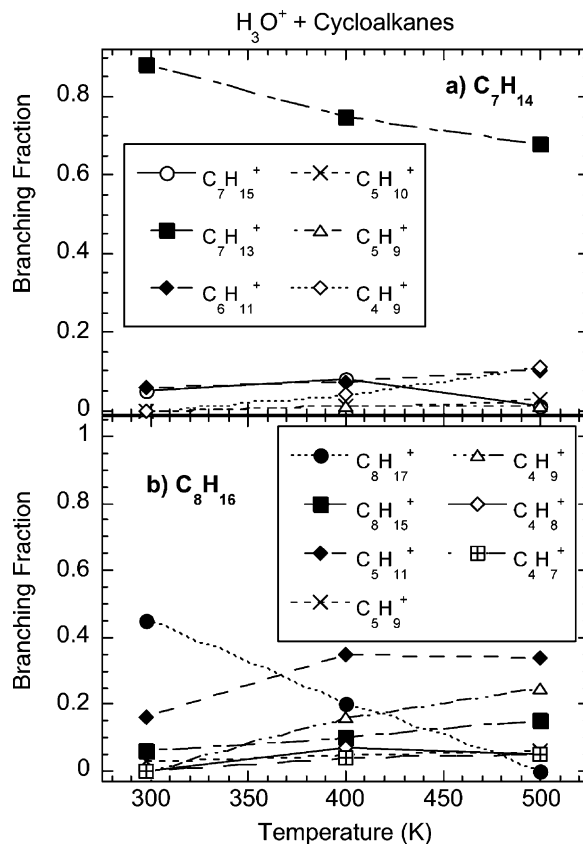


Fig. 5. (a) C_mH_n branching fractions where $m = 4-7$ for H_3O^+ reaction with C_7H_{14} vs. temperature in K measured in the VT-SIFT. (b) C_mH_n branching fractions where $m = 4-7$ for H_3O^+ reaction with C_8H_{16} vs. temperature in K measured in the VT-SIFT. The lines are shown as a guide to the eye.

ature, but the branching fraction for this channel decreases to an immeasurably small amount by 500 K. Almost one-third of the room temperature products are due to association. The association products are not observed at higher temperature and may thermally dissociate back into the initial reactants at temperatures above 298 K. The fragmentation channels that eliminate H_2 and C_3H_6 are also important and increase in abundance with increased temperature. The $C_4H_9^+$ and $C_5H_{11}^+$ ions are the major products at higher temperature and may be formed with either a secondary or tertiary structure, the latter of which would be the most stable.

The rate constants display a negative temperature dependence. The negative temperature dependence is indicative of a reaction mechanism involving complex formation and is consistent with the observation of a stable association product at 298 K for both cycloalkanes. Spanel et al. [4] have measured the rate constant for the H_3O^+ reaction with C_7H_{14} in a SIFT at 298 K to be $7 \times 10^{-10} \text{ cm}^3 \text{ s}^{-1}$ [4], which agrees well with the value of $8 \times 10^{-10} \text{ cm}^3 \text{ s}^{-1}$ measured here. The temperature dependence for the C_7H_{14} and C_8H_{16} reaction rate constants are $T^{-1.34}$ and $T^{-1.6}$, respectively.

The branching fractions observed with H_3O^+ are consistent with the energetics of the reaction in Tables 5 and 6, where the predominant channels are either exothermic or there is sufficient energy to overcome the reaction endothermicity at the temperatures studied. As with the O_2^+ and NO^+ reactions, the ionic products favored have a corresponding closed-shell aliphatic or olefinic neutral fragment.

4. Discussion

The ion chemistry of cycloalkanes investigated in this study appears quite complicated given the number and variety of reaction products observed, namely the dissociative channels. This statement holds for all three fundamental classes of ion–molecule reactions studied, namely charge transfer, hydride transfer, and proton transfer. However, examination of Figs. 2–5 and Tables 1–8, leads to the discovery of several commonalities. For example, each reaction system has one major product ion that corresponds to a channel where the loss of C_3H_6 is energetically feasible. Furthermore, several similarities exist between the current results and the chemistry of O_2^+ , NO^+ , and H_3O^+ ions reacting with *n*-alkanes [7–9,34], although the products and trends presently observed in the reactions of these ions with C_7H_{14} and C_8H_{16} are generally more diverse. The similarities and differences are discussed in the following section.

Under the current experimental conditions, the main charge-, hydride-, and proton-transfer heptyl and octyl product ions may undergo collisionally activated

Table 7

Calculated energies at 0 K and enthalpies at 298 K for C_7H_{14} using G2(MP2) in atomic units (a.u.)

	Energy (0 K)	Enthalpy (298 K)
Ion		
NO^+	–129.396355	–129.393050
O_2^+	–149.695627	–149.692322
H_3O^+	–76.588538	–76.584753
$\text{C}_7\text{H}_{13}^+$	–273.679869	–273.671198
Neutral		
HNO	–130.311739	–130.307956
O_2	–150.142065	–150.138759
H_2O	–76.330010	–76.326230
C_7H_{14}	–274.573353	–274.564998
H_2	–1.166358	–1.163053
H	–0.500000	–0.497639

$\text{C}_7\text{H}_{13}^+$ ion has an H atom missing from the ring carbon with the methyl group attached.

unimolecular decomposition at higher temperatures. Meot-Ner and Field [35] have observed that several thermalized C_7 – C_{10} carbonium ions undergo collisionally activated unimolecular decomposition with rates in the 0.9 – $20 \times 10^3 \text{ s}^{-1}$ range. Those experiments have been performed between 480 and 600 K with third-body pressures from 0.5 to 3.0 Torr. In this pressure range, the rate constants are in the “fall-off” region of unimolecular kinetics. Another relevant observation of Meot-Ner and Field [35] is that all

Table 8

Calculated energies at 0 K and enthalpies at 298 K for C_8H_{16} using DFT at the B3LYP/6-311++G(3df, 2p) level in atomic units (a.u.)

	Energy (0 K)	Enthalpy (298 K)
Ion		
NO^+	–129.578171	–129.574866
O_2^+	–149.913271	–149.909966
H_3O^+	–76.700379	–76.696596
$\text{C}_8\text{H}_{15}^+$	–313.482824	–313.474669
Neutral		
HNO	–130.510113	–130.50633
O_2	–150.37574	–150.372433
H_2O	–76.442005	–76.43917
C_8H_{16}	–314.364894	–314.355726
H_2	–1.169941	–1.166636
H	–0.502257	–0.499897

$\text{C}_8\text{H}_{15}^+$ ion has an intact C_8H_{16} ring structure with an H atom missing.

possible decompositions lead to an ionic product which is $C_4H_9^+$ or larger, i.e., ions capable of forming a tertiary carbocation, and a neutral olefin of C_3H_6 or larger. These results suggest that the decomposition of these ions are observable under our experimental conditions, and our experimental product distributions are consistent with this work.

In a previous study conducted in this laboratory, $C_8H_{17}^+$ ions produced in reactions with H_3O^+ and NO^+ with isooctane and *n*-octane appear to thermally dissociate in the VT-SIFT over the 300–500 K temperature range. This hypothesis has previously been tested by creating $C_8H_{17}^+$ ions from either isooctane or *n*-octane in the ion source, selectively injecting them into the flow tube and then monitoring the ion distribution as a function of temperature. At 300 K, all of the ion signal results from $C_8H_{17}^+$, but by 450 K, 80% of these ions had decomposed to $C_4H_9^+$ and $C_5H_{11}^+$ [8]. Dissociation of $C_8H_{17}^+$ ions has also been observed previously by Matsuoka and Ikezoe [36], and Lias et al. [37] have also reported observing dissociation of hydride transfer product ions for reactions of NO^+ with alkanes containing more than five carbon atoms.

Previous studies have shown that the rate constant for NO^+ reacting with alkanes is greatly enhanced as the number of carbon atoms and the amount of chain branching are increased [8,9]. Therefore, the fact that both C_7H_{14} and C_8H_{16} react with NO^+ at the collision rate is expected as the initial reactant has a cyclic structure. In the present study, little fragmentation is involved in the NO^+ reaction with C_7H_{14} as the only exothermic channel is hydride transfer to form HNO and $C_7H_{13}^+$, a tertiary carbocation with the cyclohexane ring intact. Dissociation is subsequently observed only at the highest temperatures studied due to the stability of the tertiary $C_7H_{13}^+$ ion. The dissociation pattern observed is consistent with the Meot-Ner and Field results for collisionally activated unimolecular decomposition of heptyl ions, i.e., both experiments produced C_3H_6 and a C_4 carbocation [35]. The most stable structure for the $C_4H_7^+$ ion is a secondary carbocation of the form $CH_3CHCH=CH_2^+$.

Likewise, the theoretical calculations performed regarding the structure of the $C_8H_{15}^+$ ion produced

in the reaction of NO^+ with C_8H_{16} indicate that the C_8H_{16} ring remains intact producing a secondary carbocation. Interestingly, $C_5H_9^+$ becomes the dominant ionic fragment at 700 K and this channel involves the production of a C_3H_6 neutral fragment. Both secondary and tertiary cationic isomers exist for $C_5H_9^+$ that are energetically similar [27]. However, the secondary structure is mechanistically easiest to produce. Again, this result is entirely consistent with a mechanism involving collisionally activated unimolecular decomposition of the $C_8H_{15}^+$ ion. The decomposition of $C_8H_{15}^+$ created from C_8H_{16} occurs at lower temperatures than $C_7H_{13}^+$ created from C_7H_{14} , most likely due to the fact that the former ion has a secondary carbocation structure while the latter ion has a tertiary carbocation structure and is more stable.

The O_2^+ reactions with both C_7H_{14} and C_8H_{16} show extensive fragmentation at all temperatures, as both reactions are associated with several very exothermic dissociative product channels. The charge-transfer products are the most abundant at 298 K and are likely formed with a large amount of internal energy due to the large exothermicity. The exothermicity along with the large amount of internal energy available as temperature increases leads to the large amounts of fragmentation observed.

It is interesting to compare the C_8H_{16} reaction with O_2^+ to that of O_2^+ with *n*-octane (C_8H_{18}) measured previously in the VT-SIFT [8]. In both reactions, the variation in the type of fragments observed is not very selective, $C_6H_n^+$, $C_5H_n^+$ and $C_4H_n^+$ ions comprise 90% of the dissociation products. Previous experiments have shown that *n*- $C_8H_{18}^+$ and *n*- $C_8H_{17}^+$ ions undergo collisionally activated unimolecular decomposition over the temperature range of 400–500 K [8,9,36], which is also likely to be occurring here. The reactions are sufficiently exothermic that ring breaking may occur directly. The lack of a strong pressure dependence on the fragmentation branching ratios as discussed in the experimental section would suggest that collisionally activated unimolecular decomposition may not be the primary factor governing the branching fractions in the reactions with O_2^+ .

The $C_6H_{11}^+$ ion accounts for a substantial fraction of the products formed in the reaction of O_2^+ with C_7H_{14} . The most stable isomeric form of the $C_6H_{11}^+$ ion is an ionized methylcyclopentyl ion with a tertiary carbocation structure [27]. However, the simplest mechanism involves CH_3 loss to leave a cyclohexyl cation. In either case, this ion appears to be stable over the temperature range studied. The other major fragment ions observed are $C_5H_m^+$ and $C_4H_m^+$ where the C_5 carbocations are slightly favored. The C_4 – C_6 fragment ions likely result from the decomposition of the non-dissociative charge-transfer product ion $C_7H_{14}^+$ with increasing temperature, but it is unclear from the present experimental data if the decomposition is truly unimolecular or collisionally activated.

The O_2^+ reaction with C_8H_{16} is similar to C_7H_{14} in many regards, i.e., the non-dissociative charge-transfer product is observed at 298 K, but $C_6H_m^+$, $C_5H_m^+$ and $C_4H_m^+$ fragments are the predominant products. The major distinction is that these reactions are generally more exothermic, and hence, more energy is available for dissociation, consistent with the numerous fragmentation channels observed. Again, it is unclear from the present experimental data alone if the decomposition is truly unimolecular or collisionally activated.

The proton-transfer reaction involving H_3O^+ and C_8H_{16} proceeds at approximately 1/5 of the collision rate at 298 K. The rate constants decrease moderately at 400 K, then level off at 500 K. The proton-transfer product formed in this reaction is the $C_8H_{17}^+$ ion, which is non-cyclic based on DFT calculations. Adding a proton to a carbon on the C_8H_{16} ring causes the adjacent C–C bond to break in $C_8H_{17}^+$, whereby the bond distance increases to over 7 Å, indicative of a very weak van der Waals interaction. The proton-transfer reaction is -63 kJ mol^{-1} exothermic, assuming that a linear secondary $C_8H_{17}^+$ carbocation forms with the heat of formation estimated by Arnold et al. [9]. Interestingly, the decomposition products currently observed at 400 and 500 K are essentially the same as those observed in the H_3O^+ and NO^+ reactions with *n*-octane reported previously [8,9], suggesting the $C_8H_{17}^+$ ion subsequently produced in the current experiments has a similar structure as

the $C_8H_{17}^+$ produced in the earlier work and is also undergoing collisionally activated unimolecular decomposition [8,9,36]. Also, the rate constants for the reaction of H_3O^+ with C_8H_{16} show similar trends with temperature as H_3O^+ with *n*-octane (C_8H_{18}), where a significant association product is observed at 298 K that disappears at 400 K and above. Note that in contrast to the case of the O_2^+ reactions with these cycloalkanes, the dissociation product channels in the H_3O^+ reaction are only slightly exothermic for the formation of the tertiary structures and slightly endothermic for the formation of the secondary structures of the $C_5H_{11}^+$ and $C_4H_9^+$ fragment ions. Therefore, collisionally activated unimolecular decomposition is the most likely candidate under these conditions.

The proton-transfer reaction involving H_3O^+ and C_7H_{14} proceeds at approximately 1/3 of the collision rate and exhibits a negative temperature dependence, which is usually associated with a reaction mechanism involving complex formation. This trend is consistent with the small amount of association product observed at 298 K. The fragment channels observed appear to reflect a competition between ring breaking and hydrogen elimination. Theoretical computations involving placing a proton on various carbon atoms on C_7H_{14} result in an energy optimized $C_7H_{13}^+$ tertiary carbocation structure with a weakly associated hydrogen molecule, i.e., the calculations show that protonated methylcyclohexane ($C_7H_{15}^+$) readily eliminates H_2 . The $C_7H_{13}^+$ ion maintains the original C_7H_{14} structure with an H^- removed from the ring carbon with the methyl group attached to it, leaving the cyclohexane ring intact.

No stable cyclic structure could be found corresponding to $C_7H_{15}^+$ so it is assumed that this product is either a linear or branched non-cyclic alkyl structure with an associated secondary or tertiary carbocation, respectively. The more stable tertiary form has been assumed in the reaction enthalpy calculated in Table 5. The $C_6H_{11}^+$ ion accounts for a small fraction of the products formed and its most likely formed by removing a CH_3 and producing a cyclohexyl cation and CH_4 . As the temperature increases, the relative branching

tends toward the C₄–C₆ fragments, again indicative of collisionally activated unimolecular decomposition of the larger C₇H_m⁺ ions. Collisionally activated unimolecular decomposition is the most likely dissociation mechanism given the energetics listed in Table 5.

Most exothermic proton-transfer reactions occur at the collision rate. Nevertheless, the two proton-transfer reactions reported here do not. This probably is a result of the rearrangement involved in forming H⁺C₇H₁₄ and H⁺C₈H₁₆ from C₇H₁₄ and C₈H₁₆. In the former reaction, proton transfer either leads to ring breaking (minor channel) or H₂ elimination with the ring intact (major channel). In the latter, the calculations show that the ring breaks. These rearrangements can lead to either energy or entropy barriers.

5. Conclusions

The ion chemistry of cycloalkanes has been investigated as a function of temperature for three fundamental classes of ion–molecule reactions: charge transfer, hydride transfer, and proton transfer. The rate constants and branching fractions for the reactions of O₂⁺, NO⁺ and H₃O⁺ with C₇H₁₄ and C₈H₁₆ have been studied as a function of temperature utilizing an HTFA and VT-SIFT up to 700 K. O₂⁺ reacts via direct dissociative charge transfer to generate a wide range of hydrocarbon ions and neutrals with both cycloalkanes. NO⁺, on the other hand, undergoes non-dissociative hydride transfer up to around 500 K, where increasing amounts of dissociation products arise from 500 to 700 K. All of the reactions of the two diatomic ions with the cycloalkanes occur at the capture collision rate. However, H₃O⁺ reacts at much less than the collision rate through dissociative proton transfer from 298 to 500 K, even though there are exothermic channels. The proton-transfer reactions involve significant rearrangement based on comparisons with previous work and new theoretical results. The involvement of a ring-breaking mechanism is the likely reason that exothermic proton-transfer reactions do not proceed at the collision rate. Future modifications to our HTFA will allow more facile examinations of the possible

isomeric forms of product ions using the selective reactivity of certain structural forms as a probe [38–40].

The fact that all of the reactions result in fragmentation at high temperatures has implications for ion-assisted combustion processes. Humid air plasmas interacting with a mixture of linear and cyclic alkanes generate product ions of the type that have been shown to participate in ionic chain reactions in combustion models including ion chemistry [17]. In addition, the reaction rate constants for the cycloalkanes studied here are in the range of the theoretically maximum rate constants for ion-dipole and ion-induced dipole capture collisions. Consequently, these reactions also provide a rapid way to initiate and maintain combustion processes.

Acknowledgements

We dedicate this paper to one of the pioneers in the field of ion chemistry, Jack Beauchamp. We would also like to thank John Williamson and Paul Mundis for technical support and Susan Arnold for helpful discussions. This work at AFRL was supported by the Air Force Office of Scientific Research (AFOSR), Task 2303EP4. A.J.M. and T.M.M. have been supported under Visidyne, Inc. contract number F19628-99-C-0069.

References

- [1] L.Q. Maurice, T. Edwards, J. Griffiths, in: *Scramjet Propulsion*, AIAA Progress in Astronautics and Aeronautics Series, 2000, p. 757.
- [2] W. Lindinger, J. Hirber, H. Paretzke, *Int. J. Mass Spectrom. Ion Process.* 129 (1993) 79.
- [3] A. Hansel, A. Jordan, R. Holzinger, P. Prazeller, W. Vogel, W. Lindinger, *Int. J. Mass Spectrom. Ion Process.* 149/150 (1995) 609.
- [4] P. Spanel, M. Pavlik, D. Smith, *Int. J. Mass Spectrom. Ion Process.* 145 (1995) 177.
- [5] P. Spanel, D. Smith, *J. Chem. Phys.* 104 (1996) 1893.
- [6] D. Smith, P. Spanel, *Int. Rev. Phys. Chem.* 15 (1996) 231.
- [7] P. Spanel, D. Smith, *Int. J. Mass Spectrom.* 181 (1998) 1.
- [8] S.T. Arnold, A.A. Viggiano, R.A. Morris, *J. Phys. Chem. A* 101 (1997) 9351.
- [9] S.T. Arnold, A.A. Viggiano, R.A. Morris, *J. Phys. Chem. A* 102 (1998) 8881.

- [10] S.T. Arnold, R.A. Morris, A.A. Viggiano, *J. Phys. Chem. A* 102 (1998) 1345.
- [11] S.T. Arnold, S. Williams, I. Dotan, A.J. Midey, R.A. Morris, A.A. Viggiano, *J. Phys. Chem. A* 103 (1999) 8421.
- [12] A.J. Midey, S. Williams, S.T. Arnold, I. Dotan, R.A. Morris, A.A. Viggiano, *Int. J. Mass Spectrom.* 195 (2000) 327.
- [13] S.T. Arnold, I. Dotan, S. Williams, A.A. Viggiano, R.A. Morris, *J. Phys. Chem. A* 104 (2000) 928.
- [14] S. Williams, A.J. Midey, S.T. Arnold, R.A. Morris, A.A. Viggiano, Y.-H. Chiu, D.J. Levandier, R.A. Dressler, M.R. Berman, *J. Phys. Chem. A* 104 (2000) 10336.
- [15] A.J. Midey, S. Williams, A.A. Viggiano, *J. Phys. Chem. A* 105 (2001) 1574.
- [16] A.J. Midey, S. Williams, S.T. Arnold, A.A. Viggiano, *J. Phys. Chem. A* (2003), in press.
- [17] S. Williams, A.J. Midey, S.T. Arnold, T.M. Miller, P.M. Bench, R.A. Dressler, Y.-H. Chiu, D.J. Levandier, A.A. Viggiano, R.A. Morris, M.R. Berman, L.Q. Maurice, C.D. Carter, *AIAA Fourth Weakly Ionized Gases Workshop*, Anaheim, CA, 2001.
- [18] D. Smith, P. Spanel, *Rapid Commun. Mass Spectrom.* 10 (1996) 1183.
- [19] P.M. Hierl, J.F. Friedman, T.M. Miller, I. Dotan, M. Mendendez-Barreto, J. Seeley, J.S. Williamson, F. Dale, P.L. Mundis, R.A. Morris, J.F. Paulson, A.A. Viggiano, *Rev. Sci. Instr.* 67 (1996) 2142.
- [20] A.A. Viggiano, R.A. Morris, F. Dale, J.F. Paulson, K. Giles, D. Smith, T. Su, *J. Chem. Phys.* 93 (1990) 1149.
- [21] S.T. Arnold, R.A. Morris, A.A. Viggiano, *J. Chem. Phys.* 103 (1995) 9242.
- [22] E.E. Ferguson, *J. Phys. Chem.* 90 (1986) 731.
- [23] D.R. Lide (Ed.), *CRC Handbook of Chemistry and Physics*, CRC Press, Boca Raton, 1996, p. 6.
- [24] S.G. Lias, J.E. Bartmess, J.F. Liebman, J.L. Holmes, R.D. Levin, W.G. Mallard, in: W.G. Mallard, P.J. Linstrom (Eds.), *NIST Chemistry WebBook*, NIST Standard Reference Database Number 69, NIST, Gaithersburg, 1998, <http://webbook.nist.gov>.
- [25] M.W. Chase Jr., *J. Phys. Chem. Ref. Data* 9 (1998) 1344.
- [26] M.J. Frisch, G.W. Trucks, H.B. Schlegel, G.E. Scuseria, M.A. Robb, J.R. Cheesman, V.G. Zakrzewski, J.J.A. Montgomery, R.E. Stratmann, J.C. Burant, S. Dapprich, J.M. Millam, A.D. Daniels, K.N. Kudin, M.C. Strain, O. Farkas, J. Tomasi, V. Barone, M. Cossi, R. Cammi, B. Mennucci, C. Pomelli, C. Adamo, S. Clifford, J. Ochterski, G.A. Petersson, P.Y. Ayala, Q. Cui, K. Morokuma, D.K. Malick, A.D. Rabuck, K. Raghavachari, J.B. Foresman, J. Cioslowski, J.V. Ortiz, B.B. Stefanov, G. Liu, A. Liashenko, P. Piskorz, I. Komaromi, R. Gomperts, R.L. Martin, D.J. Fox, T. Keith, M.A. Al-Laham, C.Y. Peng, A. Nanayakkara, C. Gonzalez, M. Challacombe, P.M.W. Gill, B. Johnson, W. Chen, M.W. Wong, J.L. Andres, C. Gonzalez, M. Head-Gordon, E.S. Replogle, J.A. Pople, *Gaussian 98*, Gaussian, Inc., Pittsburgh, PA, 1998.
- [27] S.G. Lias, J.E. Bartmess, J.F. Liebman, J.L. Holmes, R.D. Levin, W.G. Mallard, *J. Phys. Chem. Ref. Data* 17 (Suppl. 1) (1988) 1.
- [28] C. Rebick, in: L.F. Albright, L.C. Crynes, W.H. Corcoran (Eds.), *Pyrolysis: Theory and Industrial Practice*, Academic Press, New York, 1983.
- [29] J.W. Ochterski, *Thermochemistry in Gaussian*, Gaussian Inc., 2000.
- [30] L.A. Curtiss, K. Raghavachari, J.A. Pople, *J. Chem. Phys.* 98 (1993) 1293.
- [31] C.W. Bauschlicher, H. Partridge, *J. Chem. Phys.* 103 (1995) 1788.
- [32] T. Su, W.J. Chesnavich, *J. Chem. Phys.* 76 (1982) 5183.
- [33] T. Su, *J. Chem. Phys.* 89 (1988) 5355.
- [34] D. Smith, P. Spanel, *Adv. Atom. Mol. Opt. Phys.* 32 (1995) 307.
- [35] M. Meot-Ner, F.H. Field, *J. Phys. Chem.* 80 (1976) 2665.
- [36] S. Matsuoka, Y. Ikezoe, *J. Phys. Chem.* 92 (1988) 1126.
- [37] S.G. Lias, J.R. Eyler, P. Ausloos, *Int. J. Mass Spectrom. Ion Phys.* 19 (1976) 219.
- [38] D.M. Shold, *J. Am. Chem. Soc.* 100 (1978) 7915.
- [39] M. Meot-Ner (Mautner), F.H. Field, *J. Am. Chem. Soc.* 100 (1978) 1356.
- [40] S. Williams, W.B. Knighton, A.J. Midey, A.A. Viggiano, S. Irle, K. Morikuma, *J. Phys. Chem. A* (2003), submitted for publication.